Adimensional theory of shielding in ultracold collisions of dipolar rotors

Maykel L. González-Martínez, John L. Bohn, and Goulven Quéméner

Adimensional theory of shielding in ultracold collisions of dipolar rotors

Maykel L. González-Martínez,[1] John L. Bohn,[2] and Goulven Quéméner[1]

[1]*Laboratoire Aimé Cotton, CNRS, Université Paris-Sud, ENS Paris-Saclay, Université Paris-Saclay*
Bât. 505, Campus d'Orsay, 91405 Orsay, France
[2]*JILA, NIST, and Department of Physics, University of Colorado, Boulder, Colorado 80309-0440, USA*
(Dated: August 18, 2017)

We investigate the electric field shielding of ultracold collisions of dipolar rotors, initially in their first rotational excited state, using an adimensional approach. We establish a map of good and bad candidates for efficient evaporative cooling based on this shielding mechanism, by presenting the ratio of elastic over quenching processes as a function of a rescaled rotational constant $\tilde{B} = B/s_{E_3}$ and a rescaled electric field $\tilde{F} = dF/B$. B, d, F, s_{E_3} are respectively the rotational constant, the full electric dipole moment of the molecules, the applied electric field and a characteristic dipole-dipole energy. We identify two groups of bi-alkali dipolar molecules. The first group, including RbCs, NaK, KCs, LiK, NaRb, LiRb, NaCs and LiCs, is favorable with a ratio over 1000 at collision energies equal (or even higher) to their characteristic dipolar energy. The second group, including LiNa and KRb, is not favorable. More generally, for molecules well described by Hund's case b, our adimensional study provides the conditions of efficient evaporative cooling. The range of appropriate rescaled rotational constant and rescaled field is approximately $\tilde{B} \geq 10^8$ and $3.25 \leq \tilde{F} \leq 3.8$, with a maximum ratio reached for $\tilde{F} \simeq 3.4$ for a given $\tilde{B}$. We also discuss the importance of the electronic van der Waals interaction on the adimensional character of our study.

I. INTRODUCTION

Ultracold dipolar molecules have been the subject of tremendous experimental and theoretical investigations these past years. They are promising candidates for many interesting applications [1] using electromagnetic fields manipulation [2], from many-body physics [3] to ultracold controlled chemistry [4–8] from quantum information [9] to precision measurements [10]. Different kinds of ultracold dipolar molecules produced from already cold atoms exist now. They have been produced in ultracold gases with high enough densities to study their two-body interactions and collisions [11]. They can possess an electric or magnetic dipole moment so that they can be controlled by either an electric or magnetic field. These molecules can be fermionic or bosonic, chemically reactive or not, and produced in the absolute ground state or in a weakly bound state. Examples of fermionic molecules are ^{40}K^{87}Rb [12] and ^{23}Na^{40}K [13] while ^{87}Rb^{133}Cs [14, 15] and ^{23}Na^{87}Rb [16] are examples of bosonic molecules. They were produced in their absolute ground state in which they possess an electric dipole moment and can then be controlled by an electric field [17, 18]. Magnetic dipolar ultracold molecules such as Er$_2$ have also been produced in a weakly bound state. They possess a magnetic dipole moment and can be controlled with a magnetic field [19]. Dipolar molecules can also be cooled directly by laser cooling [20–29], by Sisyphus cooling [30–32] for polyatomic molecules, or by evaporative cooling [33].

However, all these molecules share the same problem: they can suffer from two-body collisional losses (quenching) whether it is due to the chemical reactivity of the molecules [34–36], inelastic collisions to lower molecular states [19], or possible collisional losses mediated by long-lived complex [37, 38]. It is then problematic to reach the quantum degeneracy of an ultracold gas of dipolar molecules. Quantum degeneracy can be reached by evaporative cooling, which was succesfully applied to obtain Bose–Einstein condensates of ultracold neutral atoms [39, 40] and degenerate Fermi gases [41]. The technique relies (at least but not only) on large two-body elastic rate coefficients for fast thermalization times and on small quenching rate coefficients for low collisional losses. Therefore, shielding the molecules from these unwanted collisional losses is absolutely essential to reach quantum degeneracy in ultracold gases.

A somewhat counter-intuitive scheme has been proposed to shield polar molecules from quenching collisions, by preparing them in their first rotationally excited state. In this state, if the electric field is tuned just above a critical value, there results an effective repulsion that keeps the molecules from changing their internal state or reacting. This has been studied for inelastic collisions [42], reactive collisions of $^1\Sigma$ molecules [43] or $^2\Sigma$ molecules [44]. In contrast with these previous works, this paper presents a systematic study using an adimensional perpective. We determine adimensional rescaled parameters that govern the dynamics of the systems, namely a rescaled rotational constant, a rescaled electric field and a rescaled collision energy. Then, all molecules are treated on equal footing with the same rescaled formalism [45–49]. We find the molecules and the range of the rescaled parameters for which the collisional loss suppression is low enough so that evaporative cooling techniques can be used efficiently to reach quantum degeneracy in ultracold gases of dipolar molecules.

The paper is organized as follows. In Sec. II we briefly recall the formalism used in the former papers [42–44] using dimensional quantities. Then we introduce the adimensional formalism based on the dipolar interaction which defines a characteristic length and energy. We ob-

tain adimensional rescaled cross sections, rate coefficients and scattering length as a function of the rescaled parameters. We present and discuss our results in Sec. III. With a single figure, one can determine the good molecular candidates for efficient evaporative cooling based on the shielding. We also discuss the importance of the electronic van der Waals interaction on the adimensional character of our study. Finally, we conclude in Sec. IV.

II. THEORY

A. Presentation of the scattering problem using dimensional quantities

We consider collisions between two species 1 and 2 of mass m_1 and m_2, in the presence of an external electric field F. The direction of the electric field is chosen as the space-fixed quantization axis. The species 1 and 2 are diatomic molecules considered in this study as dipolar rotors with permanent electric dipole moment $d_1 = d_2 = d$. The scattering Hamiltonian can be written

$$\hat{\mathcal{H}} = -\frac{\hbar^2}{2\mu} r^{-1} \frac{d^2}{dr^2} r + \frac{\hat{l}^2}{2\mu r^2} + \hat{\mathcal{H}}_1 + \hat{\mathcal{H}}_2 + \hat{\mathcal{V}}, \quad (1)$$

where $\mu = m_1 m_2/(m_1 + m_2)$ is the reduced mass for the molecule-molecule collision, r is the distance between the species' centers of mass, and $\hat{l}$ is the space-fixed operator for the orbital angular momentum between the two species. $\hat{\mathcal{H}}_1$ and $\hat{\mathcal{H}}_2$ describe the Hamiltonian of the isolated species 1 and 2, including their interactions with the applied field. $\hat{\mathcal{V}} = \hat{\mathcal{V}}_{\text{el}} + \hat{\mathcal{V}}_{\text{dip}}$ contains all interactions between the species, with contributions that include the electronic potential $\hat{\mathcal{V}}_{\text{el}}$ and the dipole-dipole interaction $\hat{\mathcal{V}}_{\text{dip}}$. In Sec. II B, Sec. II C, and Sec. II D, we will reduce the formalism to a model that consists in taking the long-range interaction of the molecules and treating the short-range interaction using an absorbing potential. The Hamiltonian for an isolated dipolar rotor is

$$\hat{\mathcal{H}}_{1,2} \equiv \hat{\mathcal{H}}_{\text{mol}} = \frac{\hat{n}^2}{2I} - \hat{d} \cdot \hat{F} = \frac{\hat{n}^2}{2I} - dF\cos\theta, \quad (2)$$

where $\hat{n}$ is the rotational angular momentum and I the moment of inertia of the dipolar rotor. The corresponding rotational constant is related to the moment of inertia by $B = \hbar^2/2I$. The angle θ corresponds to the angle between the permanent dipole moment and the electric field. The dipolar interaction is

$$\hat{\mathcal{V}}_{\text{dip}} = -\frac{\sqrt{6}}{4\pi\epsilon_0} r^{-3} \, \text{T}^2(\hat{d}_1, \hat{d}_2) \cdot \text{T}^2(\boldsymbol{u}_r), \quad (3)$$

where T^k represents a spherical tensor of rank k and $\boldsymbol{u}_r$ is a unit vector in the direction of $\boldsymbol{r}$. We do not consider the hyperfine structure of the molecules as the hyperfine coupling constants are much smaller than the rotational constant [50]. We solve the quantum-mechanical scattering problem using the coupled-channel method. The total wave function is first expanded in a set of N conveniently chosen basis functions $|i\rangle$,

$$|\Psi(r,\xi)\rangle = r^{-1} \sum_i \chi_i(r) |i\rangle, \quad (4)$$

where ξ is a collective variable including all coordinates except r, and i is the set of quantum numbers that label the basis functions. Each different combination of quantum numbers i defines a channel. We choose for the individual species the set of bare basis functions $|\alpha_{1,2}\rangle \equiv |\alpha\rangle = |n\, m_n\rangle$, so that

$$\langle\alpha|\hat{\mathcal{H}}_{\text{mol}}|\alpha'\rangle = B\, n(n+1)\, \delta_{\alpha,\alpha'} - d\, F\langle\alpha|\cos\theta|\alpha'\rangle. \quad (5)$$

The eigenfunctions of the corresponding matrix become the dressed internal states $|\tilde{\alpha}_{1,2}\rangle \equiv |\tilde{\alpha}\rangle = |\tilde{n}\, m_n\rangle$. The projection quantum number m_n remains a good quantum number while n is not. $\tilde{n}$ indicates that the dressed state $|\tilde{n}\, m_n\rangle$ has a main character in n when $F \simeq 0$, but is in general a linear combination of the bare states $|n\, m_n\rangle$. The corresponding eigenvalues of the dipolar rotors 1 and 2 in the field are $E_{\tilde{\alpha}_1}$ and $E_{\tilde{\alpha}_2}$. The basis functions are then symmetrized in terms of $|\tilde{\alpha}_{1,2}\rangle$, adding the orbital angular momentum, so that $|i\rangle$ is defined in Eq. (4) by

$$|i\rangle \equiv \frac{1}{\sqrt{2(1+\delta_{\tilde{\alpha}_1 \tilde{\alpha}_2})}} \left(|\tilde{\alpha}_1\rangle|\tilde{\alpha}_2\rangle + \eta|\tilde{\alpha}_2\rangle|\tilde{\alpha}_1\rangle\right) |l m_l\rangle. \quad (6)$$

The corresponding energy of the channel $|i\rangle$ is $E_i = E_{\tilde{\alpha}_1} + E_{\tilde{\alpha}_2}$, the energy of the two separated dipolar rotors 1 and 2 in the field. $\eta = +1$ ($\eta = -1$) corresponds to a symmetric (anti-symmetric) function with respect to permutation $\hat{P}$ of the identical species 1 and 2. The permutation operator acts on the basis function as $\hat{P}|i\rangle = \eta\,(-1)^l|i\rangle$. On the other hand, from the symmetrization principle, $\hat{P}|\Psi\rangle = \epsilon_P|\Psi\rangle$, where $\epsilon_P = +1$ for identical bosons and $\epsilon_P = -1$ for identical fermions. This condition implies from Eq. (4) that $\hat{P}|i\rangle = \epsilon_P|i\rangle$ and imposes the selection rule $\eta\,(-1)^l = \epsilon_P$. The time-independent Schrödinger equation $\hat{\mathcal{H}}|\Psi\rangle = E_{\text{tot}}|\Psi\rangle$, for the scattering wave function $|\Psi\rangle$ expanded over the dummy argument i' and for a total energy E_{tot} of the colliding system, provides a set of N by N coupled differential equations for the channel functions $\chi_{i'}(r)$ when projected onto the N possible bra $\langle i|$,

$$\langle i|(\hat{\mathcal{H}} - E_{\text{tot}})|\Psi\rangle = \sum_{i'} \langle i|(\hat{\mathcal{H}} - E_{\text{tot}})|r^{-1}\chi_{i'}(r)|i'\rangle$$
$$= 0. \quad (7)$$

Using the form of the Hamiltonian in Eq. (1), we get the following set of coupled equations,

$$\left[-\frac{\hbar^2}{2\mu}\frac{d^2}{dr^2} + \frac{\hbar^2 l(l+1)}{2\mu r^2} + E_i - E_{\text{tot}} \right] \chi_i(r)$$
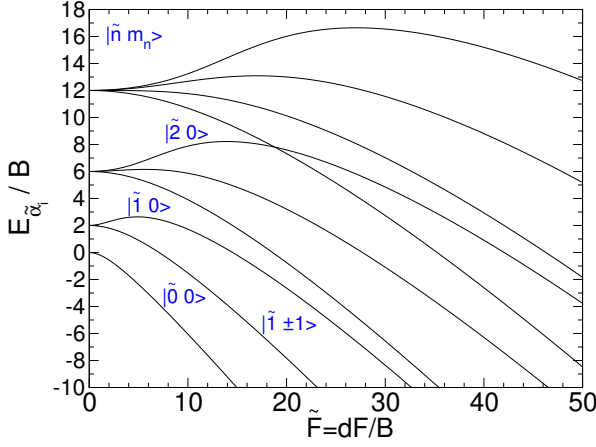$$+ \sum_{i'} V_{i,i'}(r)\, \chi_{i'}(r) = 0, \quad (8)$$

3

FIG. 1. (Color online). Rescaled energies $E_{\tilde{\alpha}_i}/B$ of a dipolar rotor as a function of the rescaled field $\tilde{F} = dF/B$. Some dressed states $|\tilde{n}_i m_{n_i}\rangle$ are explicitly indicated.
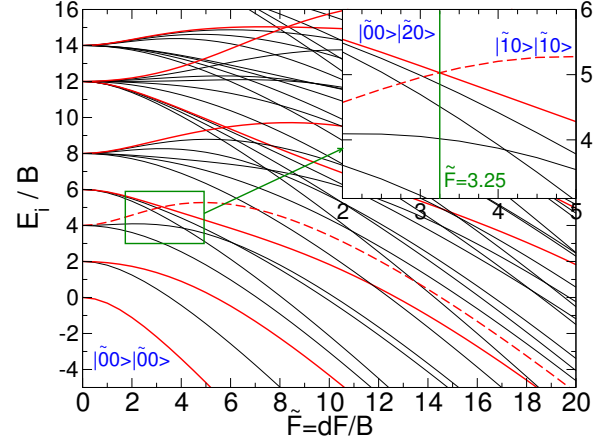

FIG. 2. (Color online). Rescaled energies E_i/B of two combined dipolar rotors as a function of the rescaled field $\tilde{F} = dF/B$. Some combined dressed states $|\tilde{n}_1 m_{n_1}\rangle|\tilde{n}_2 m_{n_2}\rangle$ are explicitly indicated. The field at which the initial state $|\tilde{1}0\rangle|\tilde{1}0\rangle$ (red bold dashed line) crosses the $|\tilde{0}0\rangle|\tilde{2}0\rangle$ one is $\tilde{F} = 3.25$. The red bold dashed and red bold solid lines correspond to states with $m_{n_1} = m_{n_2} = 0$.

where we used the notation $V_{i,i'} \equiv \langle i|\hat{\mathcal{V}}|i'\rangle$. The total energy $E_{\text{tot}} = E_{\text{init}} + E_c$ is the sum of the initial combined molecular state and the collision energy E_c. Sometimes, it is convenient to diagonalize the matrix whose elements are given by

$$\left[\frac{\hbar^2 l'(l'+1)}{2\mu r^2} + E_{i'} - E_{\text{tot}}\right]\delta_{i,i'} + V_{i,i'}(r). \quad (9)$$

The corresponding set of eigenvalues for a given r are called the adiabatic energies, and one can plot the different set of energies as a function of r. The resulting curves are a very good indication of the way the molecules interact when they approach to each other as r decreases. This is shown later in Sec. III. Each term of Eqs. (8) has dimensions of energy. We will now get rid of the dimensional character of the equations.

B. The adimensional scattering problem

The adimensional problem is set up by defining a typical characteristic length and energy from the form of the interaction. A C_n/r^n type interaction defines characteristic length and energy scales [48]

$$s_{r_n} \equiv \left(\frac{2\mu C_n}{\hbar^2}\right)^{\frac{1}{n-2}}, \; s_{E_n} \equiv \frac{\hbar^2}{2\mu s_{r_n}^2}. \quad (10)$$

As the physics of the shielding occurs due to the dipole-dipole interactions at nonzero applied electric field at a large r, the dominant and most relevant energy scale of the theory is the dipolar interaction. The matrix representation of this interaction in $\langle i|\hat{\mathcal{V}}|i'\rangle$ can be written as

$$\langle i|\hat{\mathcal{V}}_{\text{dip}}|i'\rangle = \frac{C_3}{r^3}\zeta_{i,i'}(l,l',m_l,m_l';F), \quad (11)$$

with $C_3 \equiv \frac{d^2}{4\pi\epsilon_0}$, and $\zeta_{i,i'}(l,l',m_l,m_l';F)$ being adimensional geometrical coefficients depending on the orbital angular momentum as well as the rotational angular momentum via the dressed states i, i'. We also indicated the implicit dependence of the coefficients on F. Hence, the length scale for the r^{-3} dipolar interaction term is

$$s_{r_3} \equiv \frac{2\mu C_3}{\hbar^2} = \frac{2\mu}{\hbar^2}\frac{d^2}{4\pi\epsilon_0}$$
$$= 2(\mu/\text{a.u.})(d/\text{a.u.})^2, \quad (12)$$

and the corresponding energy scale is

$$s_{E_3} \equiv \frac{\hbar^2}{2\mu s_{r_3}^2} = \frac{\hbar^6}{(2\mu)^3 (d^2/4\pi\epsilon_0)^2}$$
$$= \left[8(\mu/\text{a.u.})^3(d/\text{a.u.})^4\right]^{-1}. \quad (13)$$

This defines adimensional lengths, $\tilde{r} \equiv r/s_{r_3}$ and energies $\tilde{E} \equiv E/s_{E_3}$. If one includes only $\hat{\mathcal{V}}_{\text{dip}}$ in $\hat{\mathcal{V}}$, the rescaled coupled-channel equation for a given channel $|i\rangle$ becomes

$$\left[-\frac{d^2}{d\tilde{r}^2} + \frac{l(l+1)}{\tilde{r}^2} + \left(\frac{E_i - E_{\text{init}}}{B}\right)\tilde{B} - \tilde{E}_c\right]\chi_i(\tilde{r})$$
$$+ \sum_{i'}\left(\frac{\zeta_{i,i'}(l,l',m_l,m_l';\tilde{F})}{\tilde{r}^3}\right)\chi_{i'}(\tilde{r}) = 0. \quad (14)$$

There are as many equations as channels $|i\rangle$. The above adimensional equations display three adimensional quantities relating to the physical parameters of the colliding system. The first one,

$$\tilde{B} = \frac{B}{s_{E_3}} = \frac{8B\mu^3}{\hbar^6}\left(\frac{d^2}{4\pi\epsilon_0}\right)^2$$
$$= 8(B/\text{a.u.})(\mu/\text{a.u.})^3(d/\text{a.u.})^4, \quad (15)$$

represents the rotational constant rescaled over the dipolar energy. It depends on the rotational constant, the reduced mass and the full electric dipole moment of the system. Therefore the first parameter contains all the information of an individual dipolar rotor and is fixed for a given system. The second parameter in Eqs. (14) is

$$\frac{E_i - E_{\text{init}}}{B}. \qquad (16)$$

It represents the difference between the energy E_i of two separated dipolar rotors in channel $|i\rangle$ and the energy E_{init} of the initial state, rescaled by the rotational constant. The individual rescaled energies $E_{\tilde{\alpha}_{1,2}}/B$ are obtained directly from Eq. (5) when the equation is divided on both sides by the rotational constant B [51]. They are function of a rescaled field defined by

$$\tilde{F} = \frac{d\,F}{B}, \qquad (17)$$

and plotted in Fig. 1 as a function of $\tilde{F}$. The rescaled energies E_i/B are plotted in Fig. 2 as a function of $\tilde{F}$. In the following, as the rescaled energies, their differences, as well as the coefficients $\zeta_{i,i'}$ are fixed for a given rescaled field, the second parameter is monitored implicitely by the rescaled field $\tilde{F}$ in which the system is colliding. The third parameter in Eqs. (14),

$$\tilde{E}_c = \frac{E_c}{s_{E_3}}, \qquad (18)$$

corresponds to the collision energy rescaled over the dipolar energy. In this study, we will consider the ultracold regime so that $\tilde{E}_c \to 0$ and is fixed for a given initial state of the system. The adimensional equations depend solely on $\tilde{B}$ and $\tilde{F}$.

C. Adding the electronic van der Waals interaction

Eqs. (14) are useful to determine which parameters are the relevant ones using an adimensional perspective. However, this is possible because we have only used the dipolar interaction as the typical interaction, which defined the proper length and energy scales s_{r_3} and s_{E_3}. In practice we also have to include the electronic interaction. We use a simple long-range, isotropic description based on the leading dispersion term. The matrix representation of the electronic interaction in $\langle i|\hat{\mathcal{V}}|i'\rangle$ is then

$$\langle i|\hat{\mathcal{V}}_{\text{el}}|i'\rangle \approx \delta_{i,i'}\frac{C_6^{\text{el}}}{r^6}, \qquad (19)$$

where C_6^{el} represents the electronic van der Waals coefficient between the two dipolar rotors. It must be noted, however, that this term is not rigorously scale-free in $\tilde{r}$ for it defines a different characteristic length

$$s_{r_6} \equiv \left(\frac{2\mu}{\hbar^2}|C_6^{\text{el}}|\right)^{\frac{1}{4}} \neq s_{r_3}. \qquad (20)$$

Therefore, we cannot end up in general with a strictly adimensional study. Neglecting the electronic van der Waals term is also not possible given that in some cases the geometrical factor $\zeta_{i,i'}$ vanishes in the diagonal element of $\langle i|\hat{\mathcal{V}}_{\text{dip}}|i'\rangle$, such as for an incoming and outgoing s-wave $l = l' = 0$. However, if the electronic van der Waals term plays a negligible role in the shielding effect, the study can be considered adimensional. In practice, we don't use the adimensional coupled equations Eqs. (14) to compute the scatering properties. We instead solve the dimensional coupled equations in Eqs. (8) for a fixed electronic C_6^{el} coefficient and appropriately come back to adimensional rescaled quantities. At the end of Sec. III, we discuss in more detail for which systems the electronic van der Waals interactions play a negligible part and therefore when the study becomes adimensional.

D. Cross sections, rate coefficients and scattering length

The close-coupling equations are solved for each r from a minimum value $r_{\min}$ to a maximum value $r_{\max}$ using a log-derivative propagation method [52, 53]. At $r_{\min}$, we initialize the propagation by a complex, diagonal log-derivative matrix $\mathbf{Z}$ whose elements are given by [43]

$$Z(r = r_{\min}) =$$
$$\frac{k_{\min}(4sc\sqrt{1 - p_{\text{SR}}} - i\,p_{\text{SR}})}{c^2\left(\sqrt{1 - p_{\text{SR}}} - 1\right)^2 + s^2\left(\sqrt{1 - p_{\text{SR}}} + 1\right)^2}, \qquad (21)$$

where

$$k_{\min} = \sqrt{\frac{2\mu}{\hbar^2}\left[E_{\text{tot}} - \left(V_{i,i}(r_{\min}) + \frac{\hbar^2 l(l+1)}{2\mu r_{\min}^2}\right)\right]}, (22)$$

$c = \cos\left(k_{\min}r_{\min} + \delta_{\text{SR}}\right)$ and $s = \sin\left(k_{\min}r_{\min} + \delta_{\text{SR}}\right)$. $0 \leq p_{\text{SR}} \leq 1$ and $0 \leq \delta_{\text{SR}} \leq \pi$ are two parameters that tune the loss probability and the phase shift of the incoming flux at $r_{\min}$ [54]. This is as if we had approximated the "chemically-active" internal configuration region ($r \leq r_{\min}$) of each channel $|i\rangle$ by a square-well potential from $r = 0$ to $r = r_{\min}$, whose depth is given by

$$\frac{C_3}{r_{\min}^3}\,\zeta_{i,i} + \frac{C_6^{\text{el}}}{r_{\min}^6} + \frac{\hbar^2 l(l+1)}{2\mu r_{\min}^2}, \qquad (23)$$

and whose corresponding log-derivative is Eq. (21) at $r = r_{\min}$. At the end of the propagation, one usually obtains the scattering matrix $\mathbf{S}$ by applying asymptotic boundary conditions at $r_{\max}$ when $V_{i,i}(r = r_{\max}) \to 0$. As we start with an arbitrary complex log-derivative in Eq. (21) mimicking a phenomenological loss at short-range, it implies that the $\mathbf{S}$ matrix is not necessarily unitarity. The diagonal element of a given column determines the magnitude of the elastic process while the sum

of the off-diagonal terms determines the inelastic processes. The (positive) difference of unity with the sum of the modulus square of the elements of a matrix column determines the (phenomenological) loss processes. In our study, we do not distinguish between loss and inelastic processes, they all contribute to destruction or removal of the molecules in an experimental trap. Therefore, we consider only the quenching processes which are the sum of the inelastic and the loss processes.

As we are interested in scattering properties that are independent of the collision energy, it is then more useful to present and compute the scattering length instead of the cross sections or the rate coefficients. The s-wave scattering length becomes a constant when the wavevector $k = \sqrt{2\mu E_c/\hbar^2} \to 0$. It is defined as [55]

$$a = a_{\rm re} - i\, a_{\rm im}$$
$$= \frac{1}{i\,k}\left(\frac{1 - S_{00}(k)}{1 + S_{00}(k)}\right)\bigg|_{k\to 0}, \qquad (24)$$

with $a_{\rm im} \geq 0$. S_{00} represents the diagonal elements of the **S** matrix corresponding to the initial collisional state taken into consideration. The cross sections and rate coefficients are related to the scattering length by

$$\sigma_{\rm el} = 4\pi |a|^2 \times \Delta \qquad \sigma_{\rm qu} = \frac{4\pi\, a_{\rm im}}{k} \times \Delta \qquad (25)$$

$$\beta_{\rm el} = \frac{4\pi\hbar k |a|^2}{\mu} \times \Delta \qquad \beta_{\rm qu} = \frac{4\pi\hbar\, a_{\rm im}}{\mu} \times \Delta, \qquad (26)$$

where $\Delta = 2$ if the particles are identical and start in indistinguishable states, $\Delta = 1$ otherwise. Since we are using the dimensional equations Eqs. (8) we have to rescale the quantities so that they are adimensional. This is done by dividing the scattering length with the characteristic length s_{r_3}, $\tilde{a} = \tilde{a}_{\rm re} - i\,\tilde{a}_{\rm im} = a/s_{r_3}$. Similarly, we get the rescaled cross sections $\tilde{\sigma} = \sigma/s_{\sigma_3}$ using a characteristic cross section $s_{\sigma_3} = 4\pi s_{r_3}^2$. The rescaled rate coefficients $\tilde{\beta} = \beta/s_{\beta_3}$ are obtained by using a characteristic rate coefficient $s_{\beta_3} = s_{\sigma_3} \times s_{v_3}$, where $s_{v_3} = \hbar/\mu s_{r_3}$ corresponds to a characteristic velocity. The rescaled scattering length, cross sections and rate coefficients are now related by

$$\tilde{\sigma}_{\rm el} = |\tilde{a}|^2 \times \Delta \qquad \tilde{\sigma}_{\rm qu} = \frac{\tilde{a}_{\rm im}}{\tilde{k}} \times \Delta \qquad (27)$$

$$\tilde{\beta}_{\rm el} = \tilde{k}\,|\tilde{a}|^2 \times \Delta \qquad \tilde{\beta}_{\rm qu} = \tilde{a}_{\rm im} \times \Delta, \qquad (28)$$

where $\tilde{k} = \sqrt{\tilde{E}_c} = \sqrt{E_c/s_{E_3}} \to 0$. Note that $\tilde{k}$ is characterized via s_{E_3} by the full dipole moment of the molecule, measured in a body-fixed frame (molecular frame). In reality, what one observes in a space-fixed frame (laboratory frame) is the expectation value of the dipole moment, namely the induced dipole moment $d_{\rm ind}$, for a given applied electric field. Therefore, a more appropriate characteristic energy that quantifies the dipolar interaction between the molecules is the one using the induced dipole moment instead of the full dipole moment. This energy

depends on the applied electric field $\tilde{F}$ and characterizes the typical energy at and below which the quantum regime is reached, typically when indistinguishable bosons collide in the single partial wave $l = 0$ (s-wave) or indistinguishable fermions in the single partial wave $l = 1$ (p-wave). We note this "quantum regime" energy $E_{\rm QR}(\tilde{F})$, and the limit of validity $\tilde{k} \to 0$ above corresponds to the condition $E_c \leq E_{\rm QR}(\tilde{F})$.

Finally, an important quantity for experiments is the ratio γ of the elastic over the quenching cross section or rate coefficient. This ratio is given by

$$\gamma = \frac{\beta_{\rm el}}{\beta_{\rm qu}} = \frac{\sigma_{\rm el}}{\sigma_{\rm qu}} = \frac{|a|^2}{a_{\rm im}}\,k = \frac{|\tilde{a}|^2}{\tilde{a}_{\rm im}}\,\tilde{k}. \qquad (29)$$

This ratio determines the efficiency of the evaporative cooling technique in order to reach the quantum degeneracy of ultracold gases.

III. RESULTS AND DISCUSSION

We consider ultracold identical bosonic molecules prepared initially in the state $|\tilde{n}_1 m_{n_1}\rangle|\tilde{n}_2 m_{n_2}\rangle = |\tilde{1}0\rangle|\tilde{1}0\rangle$ (for example in the ground electronic state $X^1\Sigma^+$ and in the ground vibrational state $v = 0$). Another state $|\tilde{0}0\rangle|\tilde{2}0\rangle$ crosses the initial state at a rescaled field $\tilde{F} = 3.25$. The energy curves of these states are indicated in the inset of Fig. 2, where the initial energy $E_{\rm init}$ is indicated as a red bold dashed line. It has been shown and explained [42–44] that the quenching processes were suppressed compared to the elastic ones, slightly beyond this field. We are then interested in the molecule-molecule scattering properties around this field. We assume the worst scenario for the molecules: when the two molecules are sufficiently close to each other they disappear from the experimental trap. This can be due for example to a chemically reactive collision [35], inelastic transitions to other states, collisional losses mediated by a long-lived complex [37, 38]. In our calculations, this is satisfied when full loss $p_{\rm SR} = 1$ is invoked in Eq. (21). Thus the starting diagonal elements of the log-derivative matrix for a given channel are purely imaginary and given by $Z = -i\,k_{\min}$. Spontaneous emission of molecules in the first excited rotational state can be neglected here as the lifetimes are on the order of 10^4 s, using the formula for the Einstein coefficient of spontaneous emission. Black-body radiation driving either rotational or vibrational excitations of the molecules at room temperature can be neglected as the lifetimes are on the order of 10^2 s or more for heteronuclear alkali molecules [71]. Both types of lifetime are much longer than any other timescales of an experiment (mean collision time, evaporative cooling time, trapping time), which are on the order of the second. We used $n_{1,2} = [0 - 3]$ for the rotational basis set. We used $l = [0 - 10]$ for the partial wave basis employed in Eq. (6). As we consider initial molecules in indistinguishable states, only symmetric states with $\eta = +1$ must be taken into account
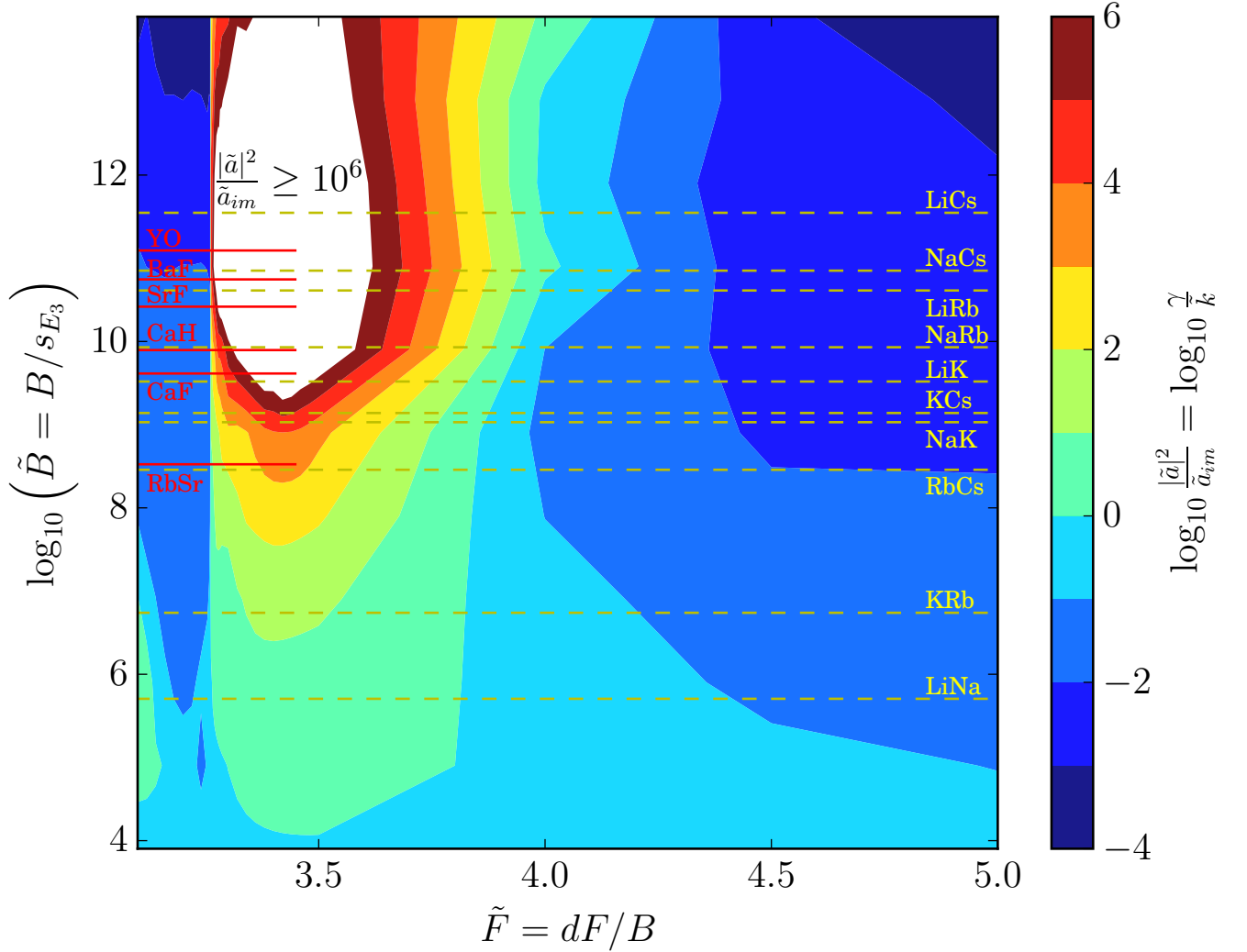
FIG. 3. (Color online). $|\tilde{a}|^2/\tilde{a}_{\mathrm{im}} \equiv \gamma/\tilde{k}$ as a function of $\tilde{B}$ and $\tilde{F}$. The color scale, presented at the right of the picture, goes from 10^{-4} to 10^6. The white area corresponds to values $\geq 10^6$. The $\tilde{B}$ values of some characteristic dipolar molecules are also included.

in Eq. (6). As we consider identical bosonic molecules, then $\varepsilon_P = +1$. The selection rules $\eta\,(-1)^l = \varepsilon_P$ implies even partial waves l. The projection quantum number $M = m_{n_1} + m_{n_2} + m_l$ of the total angular momentum on the quantization axis is conserved during the collision. We performed calculations for $M = 0$ since the initial $m_{n_1} = m_{n_2} = 0$ and $m_l = 0$ is the dominant projection at ultralow collision energies. In the following, we employ an arbitrary fixed rotational constant $B^* = 10^{-7}$ a.u. (~ 0.2 cm^{-1}) and electric dipole moment $d^* = 1$ a.u. (~ 2.54 Debye) while the mass μ^* is varied in order to vary the parameter $\tilde{B} = 8(B^*/\mathrm{a.u.})(\mu^*/\mathrm{a.u.})^3(d^*/\mathrm{a.u.})^4$ in Eq. (15). The star characterizes a hypothetical dipolar molecule, say XY*, defined by those values which also define a characteristic length $s_{r_3^*}$, energy $s_{E_3^*}$, cross section

$s_{\sigma_3^*}$, and rate coefficient $s_{\beta_3^*}$. Fixing B^* and d^* is also convenient for varying the rescaled field $\tilde{F} = d^*F/B^*$, since it is sufficient to vary the electric field F only. We consider the scattering properties at collision energies $E_c^* = 100$ nK so that the third parameter $\tilde{E}_c$ is fixed. We used $r_{\min} = 5\,a_0$ and $r_{\max}$ is chosen so that $k^*\,r_{\max}^* \sim 5$. As the mass μ^* is changed here to vary the parameter $\tilde{B}$, k^* changes accordingly, and so does $r_{\max}^*$. Most of the systems investigated in experiments are diatomic dipolar molecules of alkali atoms for which the electronic C_6^{el} coefficients belongs to the range $-20000 \leq C_6^{\mathrm{el}} \leq -3000$ a.u. [54, 56, 72, 73]. In this study we use a fixed value of $C_6^{\mathrm{el},*} = -10000$ a.u. between two molecules XY*. We discuss the effect of the C_6^{el} coefficient at the end of this section. We obtain the rescaled scattering length $\tilde{a}$ and

TABLE I. Summary of the different systems' parameters obtained from the reduced mass μ, the rotational constant B [56], and the full electric dipole moment d [57] for bosonic $^1\Sigma$ molecules and bosonic $^2\Sigma$ molecules [58–70]. $s_{r_3}, s_{E_3}, s_{\sigma_3}, s_{\beta_3}$ are respectively the characteristic length, energy, cross section and rate coefficient for the dipolar interaction (see text for definitions). $E_{QR} \simeq 3500\, s_{E_3}$ is the characteristic quantum regime energy at the field $\tilde{F} = 3.4$ where the s-wave is predominant. $\tilde{B}$ is the rescaled rotational constant. $F_{\tilde{F}=[3.25-3.8]}$ is the approximate range of the electric field where the ratio γ would be favorable for successful evaporative cooling. The systems are ordered in increasing values of $\tilde{B}$. We provide useful conversion factors: 1 a.u. $\simeq$ 1822.88 a.m.u.; 1 a.u. $\simeq$ 219475 cm^{-1}; 1 a.u. $\simeq$ 2.5417 D; 1 $a_0 \simeq 0.529 \times 10^{-10}$ m; 1 a.u. $\simeq$ 315775 K; 1 a.u. $\simeq 2.80 \times 10^{-17}$ cm^2; 1 a.u. $\simeq 6.126 \times 10^{-9}$ cm^3/s; 1 a.u. $\simeq 5.1422 \times 10^6$ kV/cm.

	μ(a.u.)	$B(10^{-7}$ a.u.)	d (a.u.)	$s_{r_3}(a_0)$	s_{E_3}(K)	E_{QR}(K) (at $\tilde{F}=3.4$)	s_{σ_3}(cm^2)	s_{β_3}(cm^3/s)	$\tilde{B}$	F(kV/cm) $\tilde{F}=[3.25-3.8]$
$^1\Sigma$										
^{7}Li^{23}Na	27349	19.4	0.200	2188	1.2×10^{-6}	4.2×10^{-3}	1.68×10^{-9}	6.16×10^{-9}	5.07×10^5	[161.8 - 189.2]
^{41}K^{87}Rb	116547	1.67	0.226	11888	9.6×10^{-9}	3.4×10^{-5}	4.97×10^{-8}	7.85×10^{-9}	5.48×10^6	[12.3 - 14.4]
^{87}Rb^{133}Cs	200349	0.77	0.49	96207	8.5×10^{-11}	3.0×10^{-7}	3.26×10^{-6}	3.70×10^{-8}	2.87×10^8	[2.64 - 3.08]
^{23}Na^{41}K	58288	4.28	1.12	146234	1.3×10^{-10}	4.4×10^{-7}	7.52×10^{-6}	1.93×10^{-7}	1.07×10^9	[6.39 - 7.47]
^{41}K^{133}Cs	158470	1.37	0.75	178279	3.1×10^{-11}	1.1×10^{-7}	1.12×10^{-5}	8.66×10^{-8}	1.38×10^9	[3.05 - 3.56]
^{7}Li^{41}K	43729	13.4	1.39	168978	1.3×10^{-10}	4.4×10^{-7}	1.01×10^{-5}	2.98×10^{-7}	3.33×10^9	[16.05 - 18.77]
^{23}Na^{87}Rb	100167	3.19	1.35	365108	1.2×10^{-11}	4.1×10^{-8}	4.69×10^{-5}	2.81×10^{-7}	8.52×10^9	[3.95 - 4.62]
^{7}Li^{87}Rb	85608	11.57	1.63	454902	8.9×10^{-12}	3.1×10^{-8}	7.28×10^{-5}	4.09×10^{-7}	4.10×10^{10}	[11.87 - 13.87]
^{23}Na^{133}Cs	142090	2.64	1.85	972605	1.2×10^{-12}	4.1×10^{-9}	3.33×10^{-4}	5.27×10^{-7}	7.10×10^{10}	[2.39 - 2.79]
^{7}Li^{133}Cs	127531	9.93	2.15	1179020	8.9×10^{-13}	3.1×10^{-9}	4.89×10^{-4}	7.12×10^{-7}	3.52×10^{11}	[7.72 - 9.03]
$^2\Sigma$										
^{87}Rb^{84}Sr	155695	0.82	0.606	114309	7.8×10^{-11}	2.7×10^{-7}	4.60×10^{-6}	5.65×10^{-8}	3.34×10^8	[2.26 - 2.65]
^{40}Ca^{19}F	53740	15.6	1.21	156797	1.2×10^{-10}	4.2×10^{-7}	8.65×10^{-6}	2.24×10^{-7}	4.12×10^9	[21.6 - 25.3]
^{40}CaH	37342	192.7	0.99	73996	7.7×10^{-10}	2.7×10^{-6}	1.92×10^{-6}	1.52×10^{-7}	7.88×10^9	[323.5 - 378.2]
^{84}Sr^{19}F	93798	11.43	1.365	349535	1.4×10^{-11}	4.8×10^{-8}	4.30×10^{-5}	2.87×10^{-7}	2.62×10^{10}	[13.99 - 16.36]
^{138}Ba^{19}F	143009	9.84	1.247	444881	5.6×10^{-12}	2.0×10^{-8}	6.97×10^{-5}	2.40×10^{-7}	5.57×10^{10}	[13.18 - 15.41]
^{89}Y^{16}O	95611	17.68	1.78	605801	4.5×10^{-12}	1.6×10^{-8}	1.29×10^{-4}	4.88×10^{-7}	1.24×10^{11}	[16.60 - 19.41]

all related quantities (see Eq. (28)) by dividing the scattering length a^* with $s_{r_3^*}$ computed for the hypothetical molecule XY*, for different values of μ^* and F^* corresponding to different values of $\tilde{B}$ and $\tilde{F}$.

The quantity $|\tilde{a}|^2/\tilde{a}_{\rm im} \equiv \gamma/\tilde{k}$ is plotted in Fig. 3 as a function of $\tilde{B}$ and $\tilde{F}$. Different contour plots are drawn from dark blue for low values of this quantity (10^{-4}) to dark red for high values (10^6). White contour plots correspond to value $\geq 10^6$. When multiplying $|\tilde{a}|^2/\tilde{a}_{\rm im}$ by the rescaled wavevector $\tilde{k}$, this provides the ratio γ for the collision energy $\tilde{E}_c$, see Eq.(28). Therefore, this plot gives directly the ratio γ for $\tilde{k} = 1$ that is when $E_c = s_{E_3}$. For efficient evaporative cooling to occur, a ratio $\gamma \geq 100$ [39], and perhaps a safer value of $\gamma \geq 1000$, is required. The latter condition corresponds in the figure to the orange, red, dark red, and white contour plots. Therefore, the condition for favorable evaporative cooling is delimited approximately by the region $\tilde{B} \geq 10^8$ and $3.25 \leq \tilde{F} \leq 3.8$, with a maximum ratio reached for $\tilde{F} \simeq 3.4$ for a given $\tilde{B}$. Any other position in the plot

is likely to be unfavorable. This universal feature is due to the shielding mechanism [42–45] when the incident collisional channel becomes repulsive enough so that the quenching rate coefficient is supressed.

The characteristic values of the dipolar bi-alkali molecules are reported in Tab. I. The $\tilde{B}$ values are reported on the right of Fig. 3 as yellow dashed lines. This distinguishes two groups of molecules for evaporative cooling, the good candidates from the bad. Group 1 (RbCs, NaK, KCs, LiK, NaRb, LiRb, NaCs, LiCs) for which $\tilde{B} > 10^8$ has favorable candidates, while group 2 (LiNa, KRb) has unfavorable ones since $\tilde{B} \ll 10^8$. This holds at collision energies $E_c = s_{E_3}$ (see Tab. I for the values), when $\tilde{k} = 1$. As mentionned in Sec. II D, a more appropriate value is when the collision energy is on the order of the quantum regime energy ($E_c = E_{QR}$) since it better reflects the magnitude of the interaction and the collision for the given applied field. Let's take the example of $\tilde{F} = 3.4$. At this field, $d_{\rm ind} \simeq 0.13\, d$ (this can be directly calculated from Fig. 1 using the slope
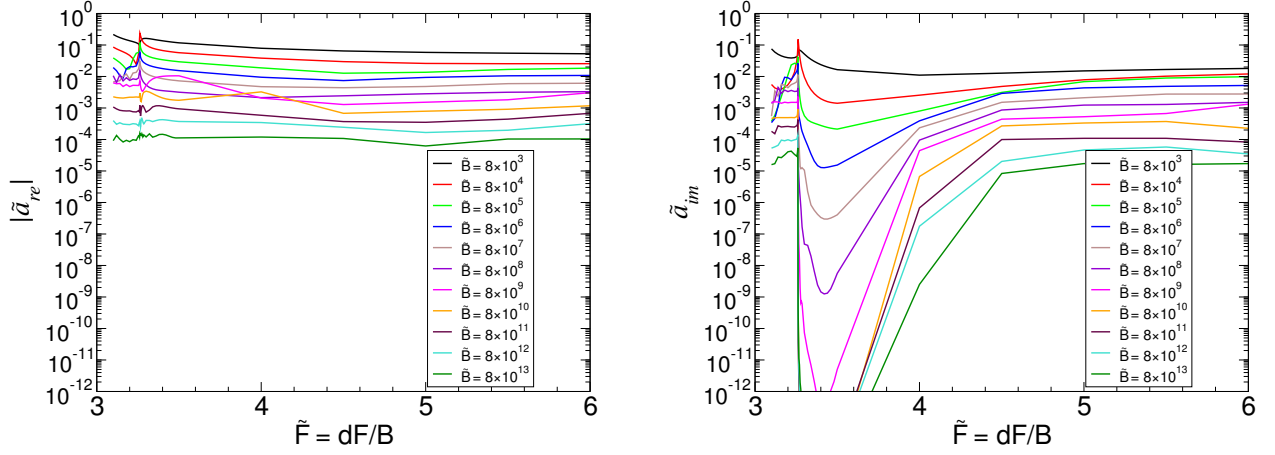
FIG. 4. (Color online). Absolute value of the real part $|\tilde{a}_{\rm re}|$ (left panel) and imaginary part $\tilde{a}_{\rm im}$ (right panel) of the rescaled scattering length as a function of $\tilde{F}$ for different values of $\tilde{B}$. The order of the curves at $\tilde{F} = 6$ corresponds to the order of the $\tilde{B}$ values displayed in the legend from top to bottom.

of the $|\tilde{1}0\rangle$ curve at $\tilde{F} = 3.4$). Then $E_{\rm QR}(\tilde{F} = 3.4) \simeq s_{E_3}/0.13^4 \simeq 3500\, s_{E_3}$. The corresponding values for each molecule are reported in Tab. I. If now $E_c = E_{QR}$, the ratio should become $\gamma(\tilde{F} = 3.4) = \tilde{k}_{QR} \times |\tilde{a}|^2/\tilde{a}_{\rm im}$ with $\tilde{k}_{QR} = \sqrt{E_{QR}/s_{E_3}} \simeq \sqrt{3500} \simeq 60$. The ratio should increase by a factor of 60 for this example compared to the one for $E_c = s_{E_3}$. The precedent conclusions remain unchanged since for the first group, the ratio γ will be bigger than 1000 while for the second group, the ratio increases by the factor of 60 but is not enough to reach the ratio of 1000.

The white contour plots in Fig. 3 correspond to values of the ratio bigger than 10^6 at $\tilde{k} = 1$. This area is not shown in more detail since we encounter numerical issues leading to unphysical oscillations in the values of the scattering quantities. In this region, the quenching processes are so strongly suppressed that the values of $\tilde{a}_{\rm im}$ compared to the ones of $|\tilde{a}_{\rm re}|$ are very tiny, about 10^{-10} smaller (see Fig. 4 below). We believe the log-derivative method cannot achieve higher precision and produces numerical errors. One can use for example more appropriate methods for better numerical precision [74] to fulfill the plot in the white area. From an experimental point of view though, the ratio presented in the figure is already more than sufficient. When $\tilde{a}_{\rm im} \ll \tilde{a}_{\rm re}$, $|\tilde{a}|^2 \simeq |\tilde{a}_{\rm re}|^2$ so that $|\tilde{a}|^2/\tilde{a}_{\rm im} \simeq |\tilde{a}_{\rm re}|^2/\tilde{a}_{\rm im}$. Since $|a_{re}|/\tilde{a}_{\rm im} \sim 10^{10}$ and $|a_{re}| \geq 10^{-4}$ (see Fig. 4), then the white area corresponds to $|\tilde{a}_{\rm re}|^2/\tilde{a}_{\rm im} \geq 10^6$.

The results in Fig. 3 are promising for bosonic dipolar molecules under current experimental interest, such as $^{87}{\rm Rb}^{133}{\rm Cs}$ [14, 15] and $^{23}{\rm Na}^{87}{\rm Rb}$ [16] since they belong to the first group as defined above. For NaRb, at $\tilde{F} \simeq 3.4$, the ratio γ reach values above 10^6 for the collision energy range from $s_{E_3} = 1.2 \times 10^{-11}$ K ($\tilde{k} = 1$) to $E_{QR} = 4.1 \times 10^{-8}$ K. This is then well appropriate to reach quantum degeneracy of ultracold dipolar gases and form Bose-Einstein condensates of dipolar

molecules. To compare with, the typical critical temperature $T_c \sim 3.3125\, \hbar^2\, n^{2/3}/mk_B$ where condensation takes place (though for a ideal non-interacting Bose gas) with a typical density of 10^{12} molecules/cm^3 is $T_c \sim 10$ nK for NaRb, which belongs to the energy range where the ratio is favorable for evaporative cooling. It should be noted that E_{QR} is not an upper limit of the collision energy above which the evaporative cooling technique would become unfavorable. The ratio can still remain big (above 1000) for even higher collision energies. It just means that one cannot strictly use Eq.(29) to convert the quantity $|\tilde{a}|^2/\tilde{a}_{\rm im}$ to the ratio γ using $\tilde{k}$. For instance for NaRb, the ratio is above 10^6 at $E_c = E_{QR}$, but it can take a high collision energy for the ratio to get down to 1000 (see Ref. [44]), so that at the $E_c \sim \mu$K regime the ratio is still favorable. To answer up to which collision energy for each system, one has then to repeat the calculation presented in Fig. 3 as a function of the collision energies. This is not shown here but can be calculated upon request (and for a specific system to save computational time). For RbCs, the ratio γ can reach values of 1000 or above for the collision energy range from $s_{E_3} = 8.5 \times 10^{-11}$ K to $E_{QR} = 3 \times 10^{-7}$ K, but at a somewhat more limited range of electric fields as shown in Fig. 3, around $\tilde{F} \simeq 3.4$. Above or below this field, the ratio can decrease and could become unfavorable.

The results of this paper are not necessarily constrained to bosonic molecules. Earlier studies [42, 43] showed that fermionic molecules also experience quenching suppression. In addition, the adimensional study and parameters remain valid, so that similar outcomes are expected for identical fermionic molecules. Examples of fermionic dipolar molecules of current experimental interest are $^{40}{\rm K}^{87}{\rm Rb}$ [12] and $^{23}{\rm Na}^{40}{\rm K}$ [13]. While fermionic KRb are not good candidates (this was shown already in Ref. [43]), we can expect that NaK will be a good candidate for quenching suppression. In contrast

with fermionic neutral particles (alkali atoms, homonuclear molecules) which interact via the van der Waals interaction at long-range, fermionic dipolar particles in an electric field interact via the dipolar interaction. This modifies the p-wave threshold laws of the elastic process [46, 75]. The elastic cross section tends to a constant at vanishing collision energies, in contrast with the van der Waals interaction where the elastic cross section vanishes as $E_c{}^2$. Since the quenching cross section behaves as $\sqrt{E_c}$, the ratio γ increases at ever lower collision energies. Therefore successful evaporative cooling can also be used to reach quantum degeneracy and form degenerate Fermi gases of dipolar molecules.

Another important experimental issue is the range of fields at which the suppression takes place, reported as $F_{\tilde{F}=[3.25-3.8]}$ in the last column of Tab. I. For example the LiNa system would require too high electric fields, above 100 kV/cm, to implement the already weak suppression. Generally in an experiment, electric fields up to ~ 5 kV/cm can be created when the electrodes stand outside the vacuum chamber [17]. Therefore, the suppression can be implemented in such circumstances for the RbCs, KCs, NaRb, NaCs systems, which require electric fields smaller than 5 kV/cm. For the remaining systems KRb, NaK, LiK, LiRb, LiCs, higher fields are required, and the electrodes must be included inside the vacuum chamber [76].

The characteristic values of representative $^2\Sigma$ dipolar molecules such as CaH, SrF, RbSr, CaF, YO, BaF, which are also of experimental interest [20–29, 77–79] are reported in Tab. I, for indication. These molecules are not perfect Hund's case b type of molecules since they have an additional fine and hyperfine structure that should be included in the Hamiltonian. Nevertheless, around the electric field $\tilde{F} = 3.25$, the electronic and nuclear spins can mainly act as spectators [44], and to same extent the formalism for $^1\Sigma$ molecules can be applied to $^2\Sigma$ molecules. The corresponding $\tilde{B}$ values, reported as red solid lines on the left of Fig. 3, show that for CaF, SrF, BaF and YO, the quantity $|\tilde{a}|^2/\tilde{a}_{\rm im}$ is well above 10^3, making them potential candidates for successful evaporative cooling under the asumption that the spins are spectators. For CaH, the electric field range is too high as for the LiNa system. For RbSr, this is like RbCs as discussed above since they share a similar value of $\tilde{B}$. γ can reach 1000 but at a restricted range of electric fields.

One cannot tell from Fig. 3 whether high ratios are due to high values of $\tilde{a}$, low values of $\tilde{a}_{\rm im}$, or a combination of both. This can be seen in Fig. 4 which shows the absolute value of the real part $|\tilde{a}_{\rm re}|$ (left) and imaginary part $\tilde{a}_{\rm im}$ (right) of the rescaled scattering length as a function of $\tilde{F}$, for different values of $\tilde{B}$, from 8×10^3 to 8×10^{13}. $|\tilde{a}_{\rm re}|$ does not vary much with $\tilde{F}$ while $\tilde{a}_{\rm im}$ does. When the field crosses the value $\tilde{F}^* = 3.25$ it strongly suppresses the quenching processes while the elastic ones remain relatively steady. The reason for the high ratio comes then from a suppressed value of $\tilde{a}_{\rm im}$ rather than an enhanced value of $|\tilde{a}_{\rm re}|$. These two plots are also useful to

have a direct magnitude of the quenching rate coefficients and elastic cross sections. $\tilde{a}_{\rm im}$ gives the quenching rate coefficients when multiplied by $s_{\beta_3} \times \Delta$ (see the values in Tab. I) while $|\tilde{a}_{\rm re}|^2$, when $\tilde{a}_{\rm im} \ll \tilde{a}_{\rm re}$, does the same for the elastic cross sections when multiplied by $s_{\sigma_3} \times \Delta$ (see Eq. (28)).
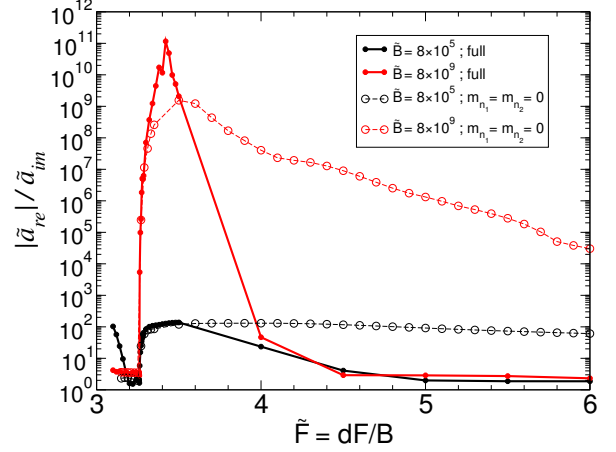

FIG. 5. (Color online). Ratio $|\tilde{a}_{\rm re}|/\tilde{a}_{\rm im}$ as a function of $\tilde{F}$ for $\tilde{B} = 8 \times 10^5$ (black thin curves) and $\tilde{B} = 8 \times 10^9$ (red bold curves). Solid curves: full calculation; dashed curves: $m_{n_1} = m_{n_2} = 0$ approximation.
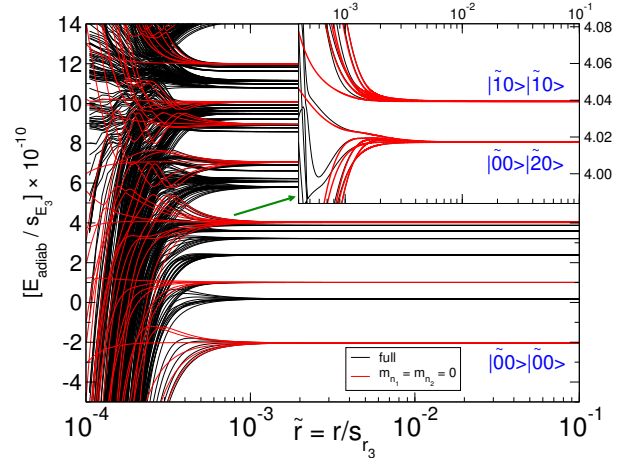

FIG. 6. (Color online). Rescaled adiabatic energies as a function of $\tilde{r}$ for $\tilde{B} = 8 \times 10^9$ and $\tilde{F} = 3.3$. Black thin curves: full calculation; red bold curves: $m_{n_1} = m_{n_2} = 0$ approximation. The inset shows a zoom of the $|\tilde{1}0\rangle|\tilde{1}0\rangle$ and $|\tilde{0}0\rangle|\tilde{2}0\rangle$ combined molecular states.

Fig. 5 confirms a useful information on the mechanism of the quenching suppression. As mentioned in Ref. [44], a useful approximation nearby $\tilde{F} = 3.25$ consists in taking only the $m_n = 0$ projection of the molecules in the calculation ($m_{n_1} = m_{n_2} = 0$). This will correspond in Fig. 2 to select only the combined molecular states indicated as red bold dashed and red bold solid lines, while a full calculation employs all the curves (red and black).
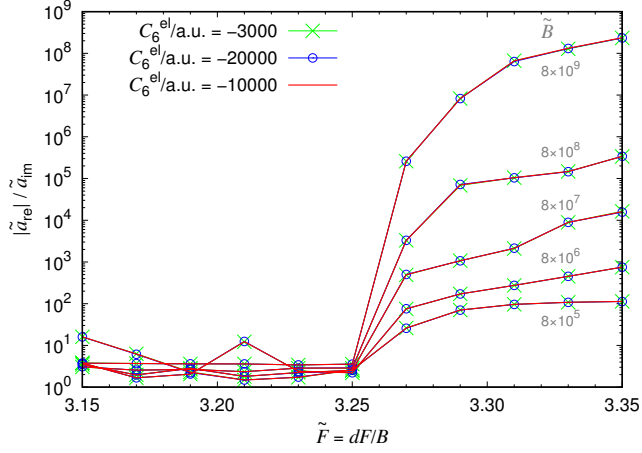
FIG. 7. (Color online). Ratio $|\tilde{a}_{\rm re}|/\tilde{a}_{\rm im}$ as a function of $\tilde{F}$ for different values of $\tilde{B}$. Solid red curves: $C_6^{\rm el,*} = -10000$ a.u. , green cross curves: $C_6^{\rm el,*} = -3000$ a.u. , blue circle curves: $C_6^{\rm el,*} = -20000$ a.u.

Fig. 5 shows the ratio $|\tilde{a}_{\rm re}|/\tilde{a}_{\rm im}$ as a function of $\tilde{F}$ for two values of $\tilde{B} = 8 \times 10^5$ and 8×10^9. The solid curves result from the full calculation, as also shown in the previous figures, while the dashed curves result from the approximation $m_{n_1} = m_{n_2} = 0$ for the rotational states of the molecules. As one can see, the approximation is valid for fields in the range $3.25 \leq \tilde{F} \leq 3.3$. For higher fields, the approximation becomes less and less valid. It strongly overestimates the results at larger fields. The approximated calculation is much faster than the full calculation as it takes much less molecular states and channels into account in the scattering, decreasing the size of the coupled equations. This can be clearly seen in Fig. 6 where the rescaled adiabatic energies have been plotted as a function of $\tilde{r}$ for the case $\tilde{B} = 8 \times 10^9$ and $\tilde{F} = 3.3$. The black thin curves corresponds to the channels used in the full calculation while the red bold curves to the channels used in the approximation. There are much less curves involved in the approximation case, yet they reproduce quite well the long-range behaviour of the fully coupled calculation, especially for the channels corresponding to the $|\tilde{1}0\rangle|\tilde{1}0\rangle$ and $|\tilde{0}0\rangle|\tilde{2}0\rangle$ combined molecular states (see inset). Therefore the approximation is really worth using at fields in the range $3.25 \leq \tilde{F} \leq 3.3$ especially due to its numerical simplicity. This range is somewhat restricted in field but even at $\tilde{F} = 3.3$ it can indicate with not much numerical effort that the suppression can be already quite strong.

Effect of the electronic van der Waals coefficient

Finally, we discuss the effect of the $C_6^{\rm el}$ coefficient. As mentioned previously in Sec. II C, the study is in general not strictly adimensional because of the van der Waals $C_6^{\rm el}/r^6$ interaction term. But to which extent this is true?

TABLE II. Van der Waals C_6 coefficients for different systems. $C_6^{\rm rot} \simeq (d/{\rm a.u.})^4/(B/{\rm a.u.})$ is the repulsive "rotational" van der Waals coefficient responsible for the repulsive interaction [43]. $C_6^{\rm el}$ is the "electronic" van der Waals coefficient, taken from [72]. The two last columns are the rescaling factor and the rescaled electronic van der Waals coefficient $C_6^{\rm el,resc.}$ from the fixed coefficient $C_6^{\rm el,*} = -10000$ a.u. used in our study (see text for details). 1 a.u. of $C_6 = 1\ E_h.a_0^6$ where E_h is a Hartree and a_0 the Bohr radius.

	$C_6^{\rm rot}$ (a.u.)	$C_6^{\rm el}$ (a.u.)	$\frac{s_{E_3} s_{r_3}^6}{s_{E_3^*} s_{r_3^*}^6}$	$C_6^{\rm el,resc.}$ (a.u.)
$^7{\rm Li}^{23}{\rm Na}$	826	-3342	0.00008	-0.8
$^{41}{\rm K}^{87}{\rm Rb}$	15623	-12636	0.0016	-16
$^{87}{\rm Rb}^{133}{\rm Cs}$	744251	-17760	0.074	-744
$^{23}{\rm Na}^{41}{\rm K}$	3673910	-7532	0.37	-3674
$^{41}{\rm K}^{133}{\rm Cs}$	2314772	-16230	0.23	-2315
$^7{\rm Li}^{41}{\rm K}$	2796249	-6689	0.28	-2796
$^{23}{\rm Na}^{87}{\rm Rb}$	10414091	-9046	1.04	-10414
$^7{\rm Li}^{87}{\rm Rb}$	6099595	-8114	0.61	-6100
$^{23}{\rm Na}^{133}{\rm Cs}$	44324439	-11998	4.43	-44324
$^7{\rm Li}^{133}{\rm Cs}$	21512044	-11007	2.15	-21512

This is what Fig. 7 answers, where the ratio $|\tilde{a}_{\rm re}|/\tilde{a}_{\rm im}$ is plotted as a function of $\tilde{F}$ for different values of $\tilde{B}$ and different values of $C_6^{\rm el,*}$. The ratio does not change for the different $C_6^{\rm el,*}$ employed. The reason can be understood as follows. There are two competing effects for the dispersion term between two XY molecules: (i) an attractive "electronic" van der Waals interaction with a negative coefficient $C_6^{\rm el}$; (ii) a "rotational" van der Waals interaction with a coefficient $C_6^{\rm rot}$ that can be tuned positive or negative depending on the electric field [43]. The former coefficients are taken from [72] between two $|\tilde{0}0\rangle$ molecules and are negative since the interaction is attractive. These coefficients constitute an upper value in magnitude for the coefficient between two $|\tilde{1}0\rangle$ molecules. The latter coefficient can be estimated semi-quantitatively by second order perturbation theory where the correction behaves as $\simeq W^2/\Delta E$. The dipolar interaction scales as $W \simeq (d^2/4\pi\varepsilon_0)/r^3$. An upper value of the difference in energy between the states $|\tilde{1}0\rangle|\tilde{1}0\rangle$ and $|\tilde{0}0\rangle|\tilde{2}0\rangle$ is approximately $\Delta E \simeq B$ for $\tilde{F} \geq 3.25$ (see Fig. 2). This provides an order of magnitude of the repulsive van der Waals interaction $\simeq (d^2/4\pi\varepsilon_0)^2/(Br^6)$ with a positive $C_6^{\rm rot} \simeq (d/{\rm a.u.})^4/(B/{\rm a.u.})$ for the initial state $|\tilde{1}0\rangle|\tilde{1}0\rangle$. Both values are reported in Tab. II. The value we use is actually not $C_6^{\rm el}$ but $C_6^{\rm el,*} = -10000$ a.u. as mentioned above for the hypothetical system XY*. This is a fixed value. However, to obtain the rescaled $C_6^{\rm el,resc.}$ coefficient for the real bi-alkali dipolar molecules, we have to rescale

$C_6^{\text{el},*}$ with a rescaling factor so that

$$C_6^{\text{el,resc.}} = C_6^{\text{el},*} \times \frac{s_{E_3} s_{r_3}^6}{s_{E_3^*} s_{r_3^*}^6}, \qquad (30)$$

which depends on the system. This is due to the fact that we use a characteristic length and energy relative to the dipolar interaction instead of the van der Waals interaction. The values of the rescaling factor and the resulting $C_6^{\text{el,resc.}}$ from $C_6^{\text{el},*} = -10000$ a.u. are reported in Tab. II. One can see that the $C_6^{\text{el,resc.}}$ coefficients are always much smaller than the C_6^{rot} ones so it will not affect the scattering quantities, as seen in Fig. 7. In that sense, the study can be considered as independent of this coefficient and then adimensional for this specific $C_6^{\text{el},*}$.

But is it appropriate to use the value $C_6^{\text{el},*} = -10000$ a.u. to describe the real molecules XY? And does it quantitatively affect the results? For the systems of group 1, although the values of $|C_6^{\text{el,resc.}}|$ do not reproduce exactly the values of the real $|C_6^{\text{el}}|$, this is still acceptable since they are much smaller than $|C_6^{\text{rot}}|$. In other words, as far as $|C_6^{\text{el}}|$ remains small compared to $|C_6^{\text{rot}}|$, the value of the scattering quantities are not going to be affected with this value of $C_6^{\text{el},*}$ employed, and the study is considered adimensional for this group. This is questionable for group 2 though, where $|C_6^{\text{el}}|$ is comparable or bigger than $|C_6^{\text{rot}}|$, and one has to be careful with the value of $C_6^{\text{el},*}$ used. One can see that the $|C_6^{\text{el,resc.}}|$ coefficients are much smaller than the real ones $|C_6^{\text{el}}|$ so that we strongly underestimate their values in our calculation. In contrast with group 1, this is not acceptable since we cannot neglect the value of $|C_6^{\text{el}}|$ compared to the value of $|C_6^{\text{rot}}|$. Therefore, the scattering quantities and the ratio γ are certainly affected and the study cannot be considered as adimensional for group 2. A systematic study is then recommended including the proper C_6^{el} coefficient. But when doing so, for KRb for instance [43], the order of magnitude of the ratio γ still remains far below 1000. Then the definition of group 1 and 2 determined above remains unchanged.

IV. CONCLUSION

In conclusion, we performed a general study on shielding ultracold dipolar rotors using an adimensional perspective, in order to identify which systems are good candidates for efficient evaporative cooling based on two-body collisions. We showed that, among the bi-alkali dipolar molecules, two groups can be distinguished. Group 1, including the molecules RbCs, NaK, KCs, LiK, NaRb, LiRb, NaCs, LiCs, is favorable for efficient evaporative cooling using the shielding mechanism as they have a ratio elastic/quenching processes over 1000 at a collision energy equal to and even higher than their characteristic dipolar energy. Group 2, including LiNa and KRb, is not favorable. In general, the study is not strictly adimensional since it contains two competing interactions, the electronic van der Waals interaction and the dipolar interaction, from which different characteristic length and energy can be defined. As we rescale the Schrödinger equation with the dipolar length and energy, the rescaled expression of the electronic van der Waals interaction breaks the adimensionality. However, the study can be considered adimensional for the first group since the electronic van der Waals coefficient is small in magnitude compared to the rotational one, responsible for the shielding. For group 2, it can not be considered adimensional as the electronic van der Waals coefficient is comparable or even bigger in magnitude compared to the rotational one, so that the electronic van der Waals coefficient we used is underestimated. A systematic study is then recommended for group 2. Despite that, the conclusions of the paper remained qualitatively unchanged.

For some molecules of group 1, large static electric fields are required to reach the shielding regime. An alternative method would consist in using electromagnetic waves such as microwaves [80, 81] to perform the suppression of quenching collisions. This will be investigated in a future work using the same time-independent quantum formalism presented here including a Floquet formalism [82, 83]. Finally, further studies could be investigated to see if a similar shielding scheme is possible for cold polyatomic molecules [30–32].

ACKNOWLEDGMENTS

[1] L. D. Carr, D. DeMille, R. V. Krems, and J. Ye, New J. Phys. **11**, 055049 (2009).

[2] M. Lemeshko, R. V. Krems, J. M. Doyle, and S. Kais, Mol. Phys. **111**, 1648 (2013).

[3] M. A. Baranov, M. Dalmonte, G. Pupillo, and P. Zoller, Chem. Rev. **112**, 5012 (2012).

[4] R. V. Krems, Phys. Chem. Chem. Phys. **10**, 4079 (2008).

[5] M. L. González-Martínez, O. Dulieu, P. Larrégaray, and L. Bonnet, Phys. Rev. A **90**, 052716 (2014).

[6] T. V. Tscherbul and R. V. Krems, Phys. Rev. Lett. **115**, 023201 (2015).

[7] A. Dóćaj, M. L. Wall, R. Mukherjee, and K. R. A. Hazzard, Phys. Rev. Lett. **116**, 135301 (2016).

[8] J. Wolf, M. Deiß, A. Krükow, E. Tiemann, B. P.

Ruzic, Y. Wang, J. P. D'Incao, P. S. Julienne, and J. Hecker Denschlag, ArXiv e-prints **1705**, 02892 (2017), arXiv:1705.02892.

[9] S. F. Yelin, D. DeMille, and R. Côté, Chapter 17 in Cold Molecules: Theory, Experiments, Applications. Edited by R. Krems, B. Friedrich, B. and W. C. Stwalley, CRC Press , 629 (2009).

[10] M. R. Tarbutt, J. J. Hudson, B. E. Sauer, and E. A. Hinds, Chapter 15 in Cold Molecules: Theory, Experiments, Applications. Edited by R. Krems, B. Friedrich, B. and W. C. Stwalley, CRC Press , 69 (2009).

[11] G. Quéméner and P. S. Julienne, Chem. Rev. **112**, 4949 (2012).

[12] K.-K. Ni, S. Ospelkaus, M. H. G. de Miranda, A. Pe'er, B. Neyenhuis, J. J. Zirbel, S. Kotochigova, P. S. Julienne, D. S. Jin, and J. Ye, Science **322**, 231 (2008).

[13] J. W. Park, S. A. Will, and M. W. Zwierlein, Phys. Rev. Lett. **114**, 205302 (2015).

[14] T. Takekoshi, L. Reichsöllner, A. Schindewolf, J. M. Hutson, C. R. Le Sueur, O. Dulieu, F. Ferlaino, R. Grimm, and H.-C. Nägerl, Phys. Rev. Lett. **113**, 205301 (2014).

[15] P. K. Molony, P. D. Gregory, Z. Ji, B. Lu, M. P. Köppinger, C. R. Le Sueur, C. L. Blackley, J. M. Hutson, and S. L. Cornish, Phys. Rev. Lett. **113**, 255301 (2014).

[16] M. Guo, B. Zhu, B. Lu, X. Ye, F. Wang, R. Vexiau, N. Bouloufa-Maafa, G. Quéméner, O. Dulieu, and D. Wang, Phys. Rev. Lett. **116**, 205303 (2016).

[17] K.-K. Ni, S. Ospelkaus, D. Wang, G. Quéméner, B. Neyenhuis, M. H. G. de Miranda, J. L. Bohn, D. S. Jin, and J. Ye, Nature **464**, 1324 (2010).

[18] M. H. G. de Miranda, A. Chotia, B. Neyenhuis, D. Wang, G. Quéméner, S. Ospelkaus, J. Bohn, J. L. Ye, and D. S. Jin, Nature Physics **7**, 502 (2011).

[19] A. Frisch, M. Mark, K. Aikawa, S. Baier, R. Grimm, A. Petrov, S. Kotochigova, G. Quéméner, M. Lepers, O. Dulieu, and F. Ferlaino, Phys. Rev. Lett. **115**, 203201 (2015).

[20] E. S. Shuman, J. F. Barry, and D. DeMille, Nature **467**, 820 (2010).

[21] J. F. Barry, D. J. McCarron, E. B. Norrgard, M. H. Steinecker, and D. DeMille, Nature **512**, 286 (2014).

[22] D. J. McCarron, E. B. Norrgard, M. H. Steinecker, and D. DeMille, New J. Phys. **17**, 035014 (2015).

[23] E. B. Norrgard, D. J. McCarron, M. H. Steinecker, M. R. Tarbutt, and D. DeMille, Phys. Rev. Lett. **116**, 063004 (2016).

[24] V. Zhelyazkova, A. Cournol, T. E. Wall, A. Matsushima, J. J. Hudson, E. A. Hinds, M. R. Tarbutt, and B. E. Sauer, Phys. Rev. A **89**, 053416 (2014).

[25] B. Hemmerling, E. Chae, A. Ravi, L. Anderegg, G. K. Drayna, N. R. Hutzler, A. L. Collopy, J. Ye, W. Ketterle, and J. M. Doyle, J. Phys. B: At. Mol. Opt. Phys. **49**, 174001 (2016).

[26] L. Anderegg, B. Augenbraun, E. Chae, B. Hemmerling, N. R. Hutzler, A. Ravi, A. Collopy, J. Ye, W. Ketterle, and J. Doyle, ArXiv e-prints **1705**, 10288 (2017), arXiv:1705.10288.

[27] M. T. Hummon, M. Yeo, B. K. Stuhl, A. L. Collopy, Y. Xia, and J. Ye, Phys. Rev. Lett. **110**, 143001 (2013).

[28] A. L. Collopy, M. T. Hummon, M. Yeo, B. Yan, and J. Ye, New J. Phys. **17**, 055008 (2015).

[29] M. Yeo, M. T. Hummon, A. L. Collopy, B. Yan, B. Hemmerling, E. Chae, J. M. Doyle, and J. Ye, Phys. Rev. Lett. **114**, 223003 (2015).

[30] M. Zeppenfeld, B. G. U. Englert, R. Glöckner, A. Prehn, M. Mielenz, C. Sommer, L. D. van Buuren, M. Motsch, and G. Rempe, Nature **491**, 570 (2012).

[31] A. Prehn, M. Ibrügger, R. Glöckner, G. Rempe, and M. Zeppenfeld, Phys. Rev. Lett. **116**, 063005 (2016).

[32] I. Kozyryev, L. Baum, K. Matsuda, B. L. Augenbraun, L. Anderegg, A. P. Sedlack, and J. M. Doyle, Phys. Rev. Lett. **118**, 173201 (2017).

[33] B. K. Stuhl, M. T. Hummon, M. Yeo, G. Quéméner, J. L. Bohn, and J. Ye, Nature **492**, 396 (2012).

[34] S. Ospelkaus, K.-K. Ni, D. Wang, M. H. G. de Miranda, B. Neyenhuis, G. Quéméner, P. S. Julienne, J. L. Bohn, D. S. Jin, and J. Ye, Science **327**, 853 (2010).

[35] P. S. Żuchowski and J. M. Hutson, Phys. Rev. A **81**, 060703 (2010).

[36] E. R. Meyer and J. L. Bohn, Phys. Rev. A **82**, 042707 (2010).

[37] M. Mayle, B. P. Ruzic, and J. L. Bohn, Phys. Rev. A **85**, 062712 (2012).

[38] M. Mayle, G. Quéméner, B. P. Ruzic, and J. L. Bohn, Phys. Rev. A **87**, 012709 (2013).

[39] E. A. Cornell and C. E. Wieman, Rev. Mod. Phys. **74**, 875 (2002).

[40] W. Ketterle, Rev. Mod. Phys. **74**, 1131 (2002).

[41] B. DeMarco and D. S. Jin, Science **285**, 1703 (1999).

[42] A. V. Avdeenkov, M. Kajita, and J. L. Bohn, Phys. Rev. A **73**, 022707 (2006).

[43] G. Wang and G. Quéméner, New J. Phys. **17**, 035015 (2015).

[44] G. Quéméner and J. L. Bohn, Phys. Rev. A **93**, 012704 (2016).

[45] J. L. Bohn, Phys. Rev. A **63**, 052714 (2001).

[46] J. L. Bohn, M. Cavagnero, and C. Ticknor, New J. Phys. **11**, 055039 (2009).

[47] C. Ticknor, Phys. Rev. A **80**, 052702 (2009).

[48] B. Gao, Phys. Rev. Lett. **105**, 263203 (2010).

[49] Y. Wang and C. H. Greene, Phys. Rev. A **85**, 022704 (2012).

[50] J. Aldegunde, B. A. Rivington, P. S. Żuchowski, and J. M. Hutson, Phys. Rev. A **78**, 033434 (2008).

[51] K. von Meyenn, Z. Phys. **231**, 154 (1970).

[52] B. R. Johnson, J. Comp. Phys. **13**, 445 (1973).

[53] D. E. Manolopoulos, J. Chem. Phys. **85**, 6425 (1986).

[54] S. Kotochigova, New J. Phys. **12**, 073041 (2010).

[55] J. M. Hutson, New J. Phys. **9**, 152 (2007).

[56] P. S. Żuchowski, M. Kosicki, M. Kodrycka, and P. Soldán, Phys. Rev. A **87**, 022706 (2013).

[57] J. N. Byrd, J. A. Montgomery, and R. Côté, Phys. Rev. A **86**, 032711 (2012).

[58] J. Chen and T. C. Steimle, J. Chem. Phys. **128**, 144312 (2008).

[59] P. S. Żuchowski, J. Aldegunde, and J. M. Hutson, Phys. Rev. Lett. **105**, 153201 (2010).

[60] R. Guérout, M. Aymar, and O. Dulieu, Phys. Rev. A **82**, 042508 (2010).

[61] T. C. Steimle, P. J. Domaille, and D. O. Harris, J. Mol. Spec. **68**, 134 (1977).

[62] W. Childs, L. Goodman, and I. Renhorn, J. Mol. Spec. **87**, 522 (1981).

[63] W. Ernst, J. Kändler, S. Kindt, and T. Törring, Chem. Phys. Lett. **113**, 351 (1985).

[64] C. Ryzlewicz and T. Törring, Chem. Phys. **51**, 329 (1980).

[65] W. E. Ernst, J. Kändler, and T. Törring, J. Chem. Phys. **84**, 4769 (1986).

[66] A. Bernard and R. Gravina, Astrophys. J. Suppl. Ser. **52**, 443 (1983).

[67] W. J. Childs, O. Poulsen, and T. C. Steimle, J. Chem. Phys. **88**, 598 (1988).

[68] R. D. Suenram, F. J. Lovas, G. T. Fraser, and K. Matsumura, J. Chem. Phys. **92**, 4724 (1990).

[69] W. J. Childs, L. S. Goodman, U. Nielsen, and V. Pfeufer, J. Chem. Phys. **80**, 2283 (1984).

[70] L. A. Kaledin, J. C. Bloch, M. C. McCarthy, and R. W. Field, J. Mol. Spectr. **197**, 289 (1999).

[71] N. Vanhaecke and O. Dulieu, Mol. Phys. **105**, 1723 (2007).

[72] M. Lepers, R. Vexiau, M. Aymar, N. Bouloufa-Maafa, and O. Dulieu, Phys. Rev. A **88**, 032709 (2013).

[73] R. Vexiau, M. Lepers, M. Aymar, N. Bouloufa-Maafa, and O. Dulieu, J. Chem. Phys. **142**, 214303 (2015).

[74] A. Simoni, A. Viel, and J.-M. Launay, J. Chem. Phys. **146**, 244106 (2017).

[75] H. R. Sadeghpour, J. L. Bohn, M. J. Cavagnero, B. D. Esry, I. I. Fabrikant, J. H. Macek, and A. R. P. Rau, J. Phys. B: At. Mol. Opt. Phys. **33**, 93 (2000).

[76] S. A. Moses, J. P. Covey, M. T. Miecnikowski, D. Jin, and J. Ye, Nature Physics **13**, 13 (2017).

[77] J. D. Weinstein, R. deCarvalho, T. Guillet, B. Friedrich, and J. M. Doyle, Nature **395**, 148 (1998).

[78] B. Pasquiou, A. Bayerle, S. M. Tzanova, S. Stellmer, J. Szczepkowski, M. Parigger, R. Grimm, and F. Schreck, Phys. Rev. A **88**, 023601 (2013).

[79] T. Chen, W. Bu, and B. Yan, Phys. Rev. A **94**, 063415 (2016).

[80] A. Micheli, G. Pupillo, H. P. Büchler, and P. Zoller, Phys. Rev. A **76**, 043604 (2007).

[81] A. V. Gorshkov, P. Rabl, G. Pupillo, A. Micheli, P. Zoller, M. D. Lukin, and H. P. Büchler, Phys. Rev. Lett. **101**, 073201 (2008).

[82] O. Atabek, R. Lefebvre, and T. Nguyen-Dang, in *Special Volume, Computational Chemistry*, Handbook of Numerical Analysis, Vol. 10 (Elsevier, 2003) p. 745.

[83] S.-I. Chu and D. A. Telnov, Phys. Rep. **390**, 1 (2004).